

MatIR: A Hybrid Mamba-Transformer Image Restoration Model

Juan Wen^{1,2}, Weiyang Hou¹, Luc Van Gool^{2,3,4}, Radu Timofte⁵

¹Zhengzhou University, ²ETH Zürich, ³KU Leuven, ⁴INSAIT, Sofia University, ⁵University of Würzburg

<https://github.com/wenjuan7275/MatIR>

Abstract

In recent years, Transformers-based models have made significant progress in the field of image restoration by leveraging their inherent ability to capture complex contextual features. Recently, Mamba models have made a splash in the field of computer vision due to their ability to handle long-range dependencies and their significant computational efficiency compared to Transformers. However, Mamba currently lags behind Transformers in contextual learning capabilities. To overcome the limitations of these two models, we propose a Mamba-Transformer hybrid image restoration model called MatIR. Specifically, MatIR cross-cycles the blocks of the Transformer layer and the Mamba layer to extract features, thereby taking full advantage of the advantages of the two architectures. In the Mamba module, we introduce the Image Inpainting State Space (IRSS) module, which traverses along four scan paths to achieve efficient processing of long sequence data. In the Transformer module, we combine triangular window-based local attention with channel-based global attention to effectively activate the attention mechanism over a wider range of image pixels. Extensive experimental results and ablation studies demonstrate the effectiveness of our approach.

1. Introduction

Image restoration aims to recover a clear and high-quality image from degraded or corrupted input. This is a long-standing problem in computer vision and encompasses a wide range of sub-problems such as super-resolution, image denoising, and deblurring. With the introduction of modern deep learning models such as CNNs [12, 16, 32, 60, 70] and Transformers [6, 8, 10, 29, 30, 54, 55], the state-of-the-art performance has been continuously improved over the past few years. Tasks such as denoising, deblurring, and super-resolution require models that can accurately reconstruct image details while preserving structural information. Traditional convolutional-based methods are often unable to capture long-range dependencies that are critical for tasks involving large or severely degraded images. Recent ad-

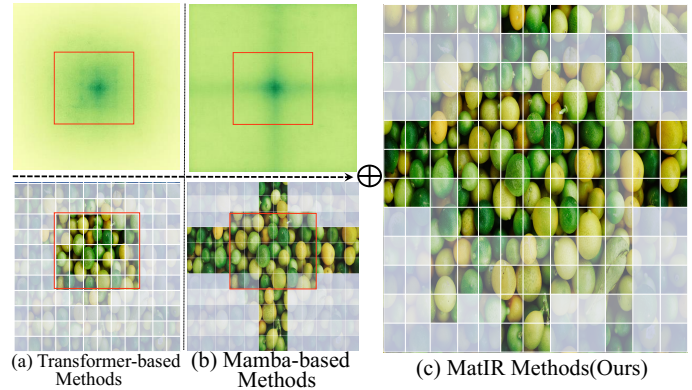


Figure 1. (a) Visualization of the effective receptive field (ERF) of the Transformer basic model [15, 35]. The figure below shows the advantage of being larger than Mamba in the context neighbor receptive field. (b) Visualization of the ERF of the Mamba basic model [33]. The figure below shows the advantage of being larger than Transformer in long sequence linear receptive fields. (c) Our proposed MatIR: A Hybrid Mamba-Transformer Image Restoration Model achieves a more significant effective receptive field.

vances in deep learning, such as the Transformer architecture, have shown promise in capturing global dependencies in images. However, the computational cost of Transformers grows quadratically with the sequence length, limiting their scalability, especially for high-resolution image restoration tasks, which offer a global receptive field at the expense of quadratic complexity.

Recently Mamba has become increasingly prominent in the field of computer vision due to its ability to manage long-distance dependencies and its significant computational efficiency relative to Transformers. The Mamba architecture is a new sequence model that achieves efficient processing of long sequence data by introducing the concept of a state space model (SSM). State-space models (SSM) leverage state-space representations to achieve linear computational complexity and can efficiently process long sequences without compromising accuracy. With linear computational complexity related to sequence length, it shows efficiency and effectiveness in handling long-distance dependencies in sequence modeling tasks. However, existing research shows that Mamba lags behind Transformers in contextual learn-

ing (ICL) capabilities. [14, 19, 50] Draw inspiration from recent advances in the development of modern deep neural networks. In this work, our aim is to compensate for the shortcomings of the models while leveraging their respective strengths. We propose a hybrid Mamba-Transformer image restoration model, called MatIR. This is a novel hybrid architecture that leverages the strengths of the Mamba architecture (known for its memory efficiency in processing long sequences) and the Transformer (excelling in contextual learning and information retrieval) [14, 19, 50]. By combining these two approaches, MatIR aims to provide a powerful and efficient solution for a variety of image restoration tasks [33, 45].

Specifically, 1) the shallow feature extraction stage uses simple convolutional layers to extract shallow features. Then 2) the deep learning feature extraction stage uses a Transformer stacked with Mamba layers. In the Transformer layer, we use triangular window local attention (TWLA) and channel global attention (CGA) to effectively activate the attention mechanism over a wider range of image pixels to improve the performance of this module. In the Mamba layer, we use the Image Restoration State Space (IRSS) module, which traverses along four scanning paths to achieve efficient processing of long sequence data from different directions and paths. The performance and throughput are improved while maintaining a manageable memory footprint. As the three core components of our MatIR, TWLA and CGA each activate more input pixels from the range of local and global, triangular window and rectangular window in attention to achieve higher quality image restoration. IRSS creates linear computational complexity information related to sequence length in the state space from four different directional paths: left, top, right, and bottom, showing efficiency and effectiveness in handling long-distance dependencies in sequence modeling tasks. Finally, 3) the high-quality image reconstruction stage aggregates shallow and deep features to produce high-quality output images. With local and global effective receptive fields as well as efficient memory management and computation, our MatIR becomes a new alternative to the image restoration backbone.

In short, our main contributions can be summarized as follows:

- We apply the state-space model and Transformer attention mechanism to the field of image restoration through extensive experiments, thus formulating MatIR, which greatly improves the computational efficiency while maintaining performance.
- We propose the Image Restoration State Space (IRSS) module, which scans and traverses along four different paths to achieve efficient processing of long sequence data.
- We propose a Triangular Window Local Attention (TWLA) block and a Channel Global Attention (CGA)

block each to attentionally activate more input pixels from the range of local and global, triangular window and rectangular window respectively in attention to achieve higher quality image restoration.

- Through comprehensive evaluation on multiple benchmark datasets, our method has superior performance compared with other state-of-the-art methods, providing a powerful and promising backbone solution for image restoration.

2. Related Work

Image Restoration. Image restoration is a long-standing problem in computer vision. In the past decade, many efforts have been made in various fields to improve the performance of deep learning methods, including image restoration. Pioneered by SRCNN [16], deep learning was introduced to image restoration super-resolution through a simple three-layer convolutional neural network (CNN). Since then, many studies have explored various architectural enhancements to improve the performance [13, 23, 24, 31, 39, 40, 42, 68, 69]. VDSR [23] implemented a deeper network, and DRCN [24] proposed a recursive structure. EDSR [31] and RDN [69] developed new residual blocks to further improve the ability of CNN in SR. However, despite the success of CNN, the receptive field of CNN is inherently limited, making it difficult to capture long-range dependencies.

In recent years, Vision Transformer (ViT) [17] and its variants [11, 34, 52] introduced the self-attention mechanism into image processing, allowing the model to learn global relationships. Based on this, IPT [6] successfully attempted to utilize transformer-based networks for various image restoration tasks. Since then, multiple techniques have been developed to enhance the performance of the image restoration Transformer. These include the shifted window self-attention implemented by SwinIR [30] and CAT [9], the grouped multiscale self-attention mechanism of ELAN [66], the sparse attention of ART [59] and OmniSR [51], and the anchored self-attention mechanism of GRL [29], the multi-attention mechanism DART, and DISR [54, 55] all of which aim to expand the range of the receptive field to achieve better results. However, it provides a global receptive field at the cost of quadratic complexity. The quadratic computational complexity of self-attention in terms of sequence length poses a challenge, especially for high-resolution images.

State Space Models. Recently, Mamba has become increasingly prominent in the field of computer vision due to its ability to manage long-distance dependencies and its significant computational efficiency relative to Transformers. The Mamba architecture is a new sequence model that achieves efficient processing of long sequence data by introducing the concept of a state space model (SSM) [14, 19, 50]. State-space models (SSM) leverage state-space representa-

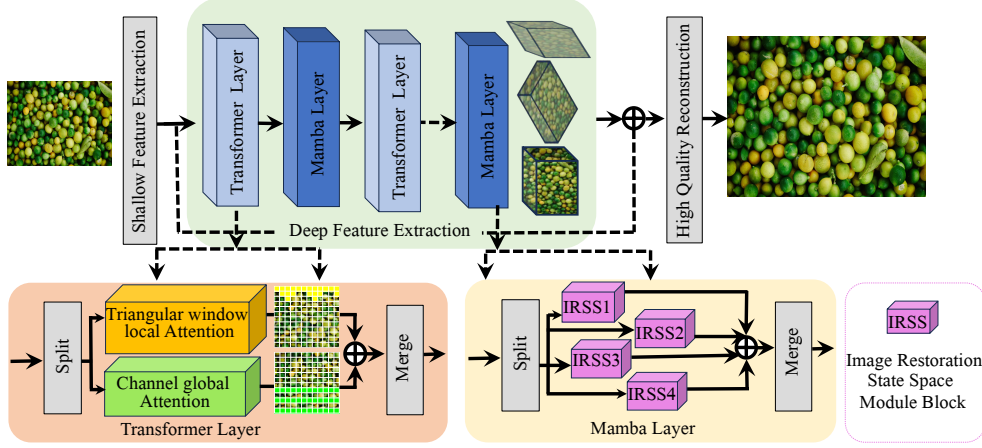


Figure 2. Overall network architecture of our MatIR.

tions to achieve linear computational complexity and can efficiently process long sequences without compromising accuracy. With linear computational complexity related to sequence length, it shows efficiency and effectiveness in handling long-distance dependencies in sequence modeling tasks. However, existing research shows that Mamba lags behind Transformers in contextual learning (ICL) capabilities [50]. The trade-off dilemma between efficient computation and global modeling has not been essentially resolved [20, 33, 45]. Considering the limitations of two current state-of-the-art models, we explore the potential of the hybrid Mamba-Transformer approach for image inpainting. In this paper, based on the effectiveness of the Mamba and Transformer models, we propose three core components, the Image Restoration State Space (IRSS) module, which scans and traverses along four different paths to achieve efficient processing of long-sequence data. The Triangular Window Local Attention (TWLA) block and the Channel Global Attention (CGA) block, each attentively activate more input pixels from the range of local and global, triangular and rectangular windows to achieve higher quality image restoration.

3. Methodology

3.1. Preliminaries

Structured state space sequence models (S4) are a recent class of sequence models for deep learning that are broadly related to RNNs, CNNs, and classical state space models. They are inspired by a particular continuous system that maps a 1-dimensional function or sequence $x(t) \in \mathbb{R} \mapsto y(t) \in \mathbb{R}$ through an implicit latent state $h(t) \in \mathbb{R}^N$.

Formally, this system can be formulated as a linear ordinary differential equation (ODE) [14, 19, 50]:

$$\begin{aligned} h'(t) &= \mathbf{A}h(t) + \mathbf{B}x(t), \\ y(t) &= \mathbf{C}h(t) + \mathbf{D}x(t), \end{aligned} \quad (1)$$

where N is the state size, $\mathbf{A} \in \mathbb{R}^{N \times N}$, $\mathbf{B} \in \mathbb{R}^{N \times 1}$, $\mathbf{C} \in \mathbb{R}^{1 \times N}$, and $\mathbf{D} \in \mathbb{R}$.

After that, the discretization process is typically adopted to integrate Eq. (1) into practical deep learning algorithms. Specifically, denote Δ as the timescale parameter to transform the continuous parameters \mathbf{A} , \mathbf{B} to discrete parameters $\bar{\mathbf{A}}$, $\bar{\mathbf{B}}$. The commonly used method for discretization is the zero-order hold rule (ZOH), which is defined as follows:

$$\begin{aligned} \bar{\mathbf{A}} &= \exp(\Delta\mathbf{A}), \\ \bar{\mathbf{B}} &= (\Delta\mathbf{A})^{-1}(\exp(\Delta\mathbf{A}) - \mathbf{I}) \cdot \Delta\mathbf{B}. \end{aligned} \quad (2)$$

After the discretization, the discretized version of Eq. (1) with step size Δ can be rewritten in the following RNN form:

$$\begin{aligned} h_k &= \bar{\mathbf{A}}h_{k-1} + \bar{\mathbf{B}}x_k, \\ y_k &= \mathbf{C}h_k + \mathbf{D}x_k. \end{aligned} \quad (3)$$

Furthermore, Eq. (3) can also be mathematically equivalently transformed into the following CNN form:

$$\begin{aligned} \bar{\mathbf{K}} &\triangleq (\mathbf{C}\bar{\mathbf{B}}, \mathbf{C}\bar{\mathbf{A}}\bar{\mathbf{B}}, \dots, \mathbf{C}\bar{\mathbf{A}}^{L-1}\bar{\mathbf{B}}), \\ \mathbf{y} &= \mathbf{x} * \bar{\mathbf{K}}, \end{aligned} \quad (4)$$

where L is the length of the input sequence, $*$ denotes the convolution operation, and $\bar{\mathbf{K}} \in \mathbb{R}^L$ is a structured convolution kernel.

Commonly, the model uses the convolutional mode Eq. (4) for efficient parallelizable training (where the whole input sequence is seen ahead of time) and switched into recurrent mode Eq. (3) for efficient autoregressive inference (where the inputs are seen one timestep at a time). An important property that we can see from the equation is that the dynamics of the model remain constant over time. This property is called linear time invariance. From this attribute, we can see the advantage of its model dynamics with Transformer, Transformer which increases quadratically with the computational cost and sequence length. The state-space model (SSM) utilizes state-space representation to achieve linear computational complexity, which has linear computational complexity related to the sequence length and can efficiently process long sequences without affecting accuracy.

3.2. Channel Global Attention Block

Recent block designs in Transformer-based restoration networks, such as those used in SwinIR, GRL, DART, and DISR [28, 30, 54, 55], have demonstrated that channel-based global attention (CGA) performs exceptionally well in the field of image restoration. This suggests that applying CGA to a MatIR-based restoration network, by tailoring a novel block structure, holds great potential. So we input the data, Let the input feature map be $\mathbf{X} \in \mathbb{R}^{C \times H \times W}$, where C is the number of channels, H, W are the spatial dimensions of the feature map. Flatten the input X along the channel dimension to obtain $\mathbf{X}_{\text{flat}} \in \mathbb{R}^{C \times N}$, where $N = H \times W$. Perform global pooling over the spatial dimensions to aggregate spatial information, obtaining a global representation for each channel: $\mathbf{z} = \frac{1}{N} \sum_{i=1}^N \mathbf{X}_{\text{flat}}[:, i]$, where $\mathbf{z} \in \mathbb{R}^C$ represents the global description for each channel. The attention mechanism directs computational resources toward the most information-rich parts of the input signal, enhancing model efficiency. The Transformer attention mechanism is based on Query(Q), Key(K) and Value(V) :

$$\text{Attention}(\mathbf{Q}, \mathbf{K}, \mathbf{V}) = \text{softmax} \left(\frac{\mathbf{Q}\mathbf{K}^\top}{\sqrt{d_k}} \right) \mathbf{V}. \quad (5)$$

In channel attention, we focus on the channel dimension and define: Query: $\mathbf{Q} = \mathbf{W}_q \mathbf{z}$, Key: $\mathbf{K} = \mathbf{W}_k \mathbf{z}$, Value: $\mathbf{V} = \mathbf{W}_v \mathbf{z}$, where $\mathbf{W}_q, \mathbf{W}_k, \mathbf{W}_v \in \mathbb{R}^{C \times C}$ are learnable weight matrices. Specifically, the channel-based global attention mechanism operates across feature dimensions, allowing us to understand which features the model relies on when making a specific decision. By analyzing the attention weights across channels, we can gain insight into the model's reasoning process, which can help identify biases or areas for improvement. So we calculate the channel attention matrix

$$\mathbf{A} = \text{softmax} \left(\frac{\mathbf{Q}\mathbf{K}^\top}{\sqrt{C}} \right), \quad (6)$$

where $\mathbf{A} \in \mathbb{R}^{C \times C}$ is the attention weight matrix between channels. The output is obtained by weighting the channel representations: $\mathbf{z}_{\text{out}} = \mathbf{A}\mathbf{V}$. Reapply the channel attention result to the original input feature \mathbf{X} , usually through dot product or channel-by-channel weighting: $\mathbf{X}_{\text{CGA}}[:, i] = \mathbf{z}_{\text{out}} \odot \mathbf{X}_{\text{flat}}[:, i]$ where \odot denotes element-wise multiplication. The final Transformer-based channel global attention formula can be simplified to $\mathbf{X}_{\text{CGA}} = \mathbf{X} \odot \text{Attention}(\mathbf{W}_q \mathbf{z}, \mathbf{W}_k \mathbf{z}, \mathbf{W}_v \mathbf{z})$. This mechanism captures the global dependencies between channels through self-attention, which helps enhance the model's understanding of multi-channel features. However, when CGA extracts features through a rectangular window, the model may experience boundary distortion and encounter limitations in the shifted configuration. Addressing these challenges can further improve the effectiveness of CGA in repairing networks.

3.3. Triangular Window Local Attention Block

In computer vision, the properties of a pixel depend on itself and its neighbors. Therefore, during self-attention, the edge pixels of the rectangular window are not explored as effectively as the internal pixels, resulting in boundary distortion. When implemented separately, the above problems are obvious in both rectangular and triangular windows [45]. Therefore, to solve the limitation of CGA introduced by MatIR, we adopted a triangular attention window in MatIR to extract features in a local range. Assume the input feature is $\mathbf{X} \in \mathbb{R}^{N \times D}$, Where: N is the number of input features, D is the dimension of the feature. We also assume that each point i has k neighbors in its local area, forming a triangular structure. For each point i , select its local k neighbors to form a local area. The triangular local structure contains the following information: Center Point X_i , Neighborhood set $\{X_j\}_{j \in \mathcal{N}(i)}$, The geometric relationships that make up a triangle, such as edge vectors and angle information: Edge Vector $e_{ij} = X_j - X_i$, Angle information: Determined by the relationship between neighbors, for example, θ_{ijk} represents the angle between j, k . In order to utilize the triangle geometric structure information, the edge feature map is designed $f_{ij} = \phi(e_{ij})$ Where θ is the multi-layer perceptron (MLP) feature mapping function; Design a triangle feature map: $f_{ijk} = \psi(e_{ij}, e_{ik}, \theta_{ijk})$ Where ψ is the triangle feature mapping function, combining two edge vectors e_{ij}, e_{ik} and angle information θ_{ijk} , Complete the triangular local feature modeling. Triangle local attention weight calculation.

$$A_{ij} = \text{Softmax} \left(\frac{Q_i K_j^T}{\sqrt{D}} + G_{ij} \right), \quad (7)$$

Finally, the triangle local feature aggregation is performed

$$Y_i = \sum_{j \in \mathcal{N}(i)} \sum_{k \in \mathcal{N}(j)} G_{ijk} A_{ij} V_j. \quad (8)$$

The local relationship is modeled through the triangle structure, emphasizing the geometric information between points and neighbors, and the computational complexity is reduced compared to global attention.

Finally, we concatenate the rectangular window-based CGA with our proposed triangular TWLA and seamlessly combine them in a Transformer Layer to further improve the performance of image restoration MatIR. The advantage of designing the Transformer layer in this way is that the model can activate more input pixels from the local and global, triangular attention window and rectangular attention window range to achieve higher quality image restoration.

3.4. Image Restoration State Space Block

The computational cost of the Transformer attention mechanism grows quadratically with the sequence length, which limits their scalability, especially for high-resolution image restoration tasks. The state-space model (SSM) uses state-space representation to achieve linear computational

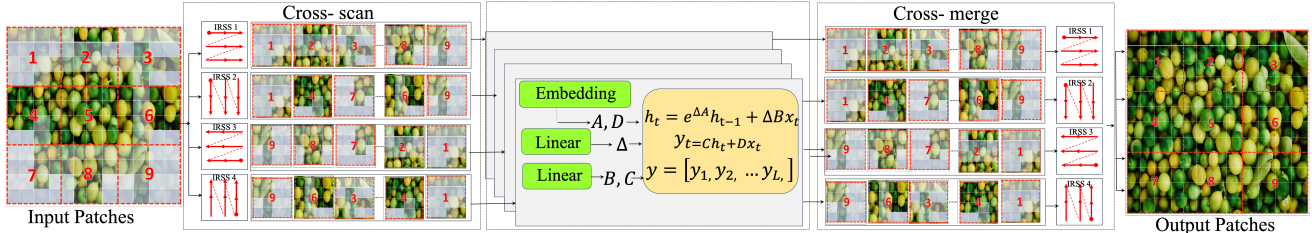


Image Restoration State Space Module Block (IRSS)

Figure 3. More details on IRSS, the core component of our MatIR model.

complexity, which can efficiently process long sequences without compromising accuracy. Inspired by these characteristics, we introduced the image restoration state-space module in the restoration model design (see 3.1 and Fig. 3), and in order to maximize the performance of this module, IRSS creates linear computational complexity information related to the sequence length in the state space from four different directional paths: left, top, right, and bottom. The designed IRSS block acts as an independent Mamba layer of the MatIR model to interact with the Transformer layer.

3.5. MatIR Overall Architecture

As shown in Fig. 2, our MatIR consists of three stages: shallow feature extraction, deep feature extraction, and high-quality reconstruction. Given a low-quality (LQ) input image $I_{LQ} \in \mathbb{R}^{H \times W \times 3}$, we first employ a 3×3 convolution layer from the shallow feature extraction to generate the shallow feature $F_S \in \mathbb{R}^{H \times W \times C}$, where H and W represent the height and width of the input image, and C is the number of channels. Subsequently, the shallow feature F_S undergoes the deep feature extraction stage to acquire the deep feature $F_D^l \in \mathbb{R}^{H \times W \times C}$ at the l -th layer, $l \in \{1, 2, \dots, L\}$. The deep learning feature extraction stage uses Transformer and Mamba stacked layers. In the Transformer layer, we use triangular window-based local attention (TWLA) and channel-based global attention (CGA) to effectively activate the attention mechanism within a wider range of image pixels to improve the performance of this module. In the Mamba layer, we use the Image Inpainting State Space (IRSS) module, which traverses along four scan paths to achieve efficient processing of long sequence data from different directions and paths. Improves performance and throughput while maintaining a manageable memory footprint. As the three core components of our MatIR, TWLA and CGA each attentively activate more input pixels from the range of local and global, triangular and rectangular windows to achieve higher quality image recovery. IRSS creates linear computational complexity information related to the sequence length in the state space from four different direction paths: left, up, right, and down. It shows efficiency and accuracy in handling long-distance dependencies in sequence modeling tasks. Effect. Finally, we use the element-wise sum to obtain the input of the high-quality reconstruction stage $F_R = F_D^L + F_S$, which is used to reconstruct the high-quality (HQ) output image

Table 1. Ablation experiments for different design choices of MatIR.

settings	Set5	Set14	Urban100
(1)remove TWLA	38.65	35.11	35.07
(2)remove CGA	38.69	35.13	35.06
(3)remove IRSS	38.67	35.12	35.08

Table 2. Model size and computational burden comparisons between MatIR and recent state-of-the-art methods.

Model	Params	FLOPs	Urban100		Manga109	
			PSNR	SSIM	PSNR	SSIM
CAT-A	16.6M	360G	27.89	0.8339	32.39	0.9285
HAT	20.8M	412G	27.97	0.9368	32.48	0.9292
ATD	20.3M	417G	28.17	0.8404	32.63	0.9306
MatIR	19.2M	398G	28.57	0.8434	32.93	0.9356

Table 3. Running time of different methods. *-T: T timesteps.

Methods	CAT-A [9]	HAT [7]	ATD [50]	Ours-10	Ours-15	Ours-20
Time (s)	15.58	15.53	15.55	15.32	17.63	22.18
PSNR↑	38.45	38.39	38.44	38.58	39.25	39.47

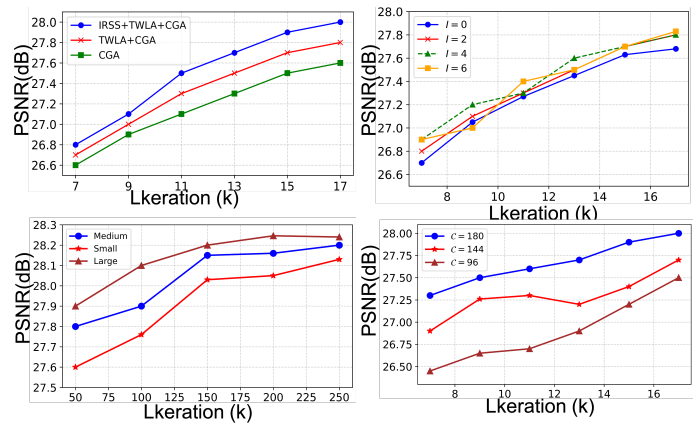


Figure 4. Comparison of iterative performance (PSNR in dB) of the proposed MatIR **Top-Left:** Performance comparison of triangle local attention, channel global attention and image recovery space modules. **Top-Right:** Triangle local attention and channel global attention, various interval sizes, **Bottom-left:** Different channel lengths. [On BSD100($\times 4$), epoch 70] and **bottom-right:** Performance evaluation of small, medium and large MatIR models.

I_{HQ} .

4. Experiments

4.1. Experiment settings.

Dataset and Evaluation. Following the setup in previous works [30, 59], we conduct experiments on various image

Table 4. Quantitative comparison on **classic image super-resolution** with state-of-the-art methods. Best results are highlighted as **first**, **second** and **third**.

Method	scale	Set5		Set14		BSDS100		Urban100		Manga109	
		PSNR	SSIM	PSNR	SSIM	PSNR	SSIM	PSNR	SSIM	PSNR	SSIM
EDSR [32]	×2	38.11	0.9602	33.92	0.9195	32.32	0.9013	32.93	0.9351	39.10	0.9773
RCAN [67]	×2	38.27	0.9614	34.12	0.9216	32.41	0.9027	33.34	0.9384	39.44	0.9786
SAN [12]	×2	38.31	0.9620	34.07	0.9213	32.42	0.9028	33.10	0.9370	39.32	0.9792
HAN [43]	×2	38.27	0.9614	34.16	0.9217	32.41	0.9027	33.35	0.9385	39.46	0.9785
IGNN [71]	×2	38.24	0.9613	34.07	0.9217	32.41	0.9025	33.23	0.9383	39.35	0.9786
CSNLN [39]	×2	38.28	0.9616	34.12	0.9223	32.40	0.9024	33.25	0.9386	39.37	0.9785
NLSA [41]	×2	38.34	0.9618	34.08	0.9231	32.43	0.9027	33.42	0.9394	39.59	0.9789
ELAN [66]	×2	38.36	0.9620	34.20	0.9228	32.45	0.9030	33.44	0.9391	39.62	0.9793
IPT [6]	×2	38.37	-	34.43	-	32.48	-	33.76	-	-	-
SwinIR [30]	×2	38.42	0.9623	34.46	0.9250	32.53	0.9041	33.81	0.9427	39.92	0.9797
SRFormer [72]	×2	38.51	0.9627	34.44	0.9253	32.57	0.9046	34.09	0.9449	40.07	0.9802
CAT-A [9]	×2	38.51	0.9626	34.78	0.9265	32.59	0.9047	34.26	0.9440	40.10	0.9805
MambaIR [20]	×2	38.57	0.9627	34.67	0.9261	32.58	0.9048	34.15	0.9446	40.28	0.9806
HAT [7]	×2	38.63	0.9630	34.86	0.9274	32.62	0.9053	34.45	0.9466	40.26	0.9809
ATD [65]	×2	38.61	0.9629	34.95	0.9276	32.65	0.9056	34.70	0.9476	40.37	0.9810
GRL [28]	×2	38.67	0.9647	35.08	0.9303	32.67	0.9087	35.06	0.9505	40.67	0.9818
MatIR (Ours)	×2	38.70	0.9648	35.13	0.9304	32.73	0.9048	35.11	0.9507	40.33	0.9806
EDSR [32]	×3	34.65	0.9280	30.52	0.8462	29.25	0.8093	28.80	0.8653	34.17	0.9476
RCAN [67]	×3	34.74	0.9299	30.65	0.8482	29.32	0.8111	29.09	0.8702	34.44	0.9499
SAN [12]	×3	34.75	0.9300	30.59	0.8476	29.33	0.8112	28.93	0.8671	34.30	0.9494
HAN [43]	×3	34.75	0.9299	30.67	0.8483	29.32	0.8110	29.10	0.8705	34.48	0.9500
IGNN [71]	×3	34.72	0.9298	30.66	0.8484	29.31	0.8105	29.03	0.8696	34.39	0.9496
CSNLN [39]	×3	34.74	0.9300	30.66	0.8482	29.33	0.8105	29.13	0.8712	34.45	0.9502
NLSA [41]	×3	34.85	0.9306	30.70	0.8485	29.34	0.8117	29.25	0.8726	34.57	0.9508
ELAN [66]	×3	34.90	0.9313	30.80	0.8504	29.38	0.8124	29.32	0.8745	34.73	0.9517
IPT [6]	×3	34.81	-	30.85	-	29.38	-	29.49	-	-	-
SwinIR [30]	×3	34.97	0.9318	30.93	0.8534	29.46	0.8145	29.75	0.8826	35.12	0.9537
SRformer [72]	×3	35.02	0.9323	30.94	0.8540	29.48	0.8156	30.04	0.8865	35.26	0.9543
CAT-A [9]	×3	35.06	0.9326	31.04	0.8538	29.52	0.8160	30.12	0.8862	35.38	0.9546
MambaIR [20]	×3	35.08	0.9323	30.99	0.8536	29.51	0.8157	29.93	0.8841	35.43	0.9546
HAT [7]	×3	35.07	0.9329	31.08	0.8555	29.54	0.8167	30.23	0.8896	35.53	0.9552
ATD [65]	×3	35.11	0.9330	31.13	0.8556	29.57	0.8176	30.46	0.8917	35.63	0.9558
MatIR (Ours)	×3	35.13	0.9328	31.06	0.8555	29.56	0.8163	30.23	0.8888	35.47	0.9551
EDSR [32]	×4	32.46	0.8968	28.80	0.7876	27.71	0.7420	26.64	0.8033	31.02	0.9148
RCAN [67]	×4	32.63	0.9002	28.87	0.7889	27.77	0.7436	26.82	0.8087	31.22	0.9173
SAN [12]	×4	32.64	0.9003	28.92	0.7888	27.78	0.7436	26.79	0.8068	31.18	0.9169
HAN [43]	×4	32.64	0.9002	28.90	0.7890	27.80	0.7442	26.85	0.8094	31.42	0.9177
IGNN [71]	×4	32.57	0.8998	28.85	0.7891	27.77	0.7434	26.84	0.8090	31.28	0.9182
CSNLN [39]	×4	32.68	0.9004	28.95	0.7888	27.80	0.7439	27.22	0.8168	31.43	0.9201
NLSA [41]	×4	32.59	0.9000	28.87	0.7891	27.78	0.7444	26.96	0.8109	31.27	0.9184
ELAN [66]	×4	32.75	0.9022	28.96	0.7914	27.83	0.7459	27.13	0.8167	31.68	0.9226
IPT [6]	×4	32.64	-	29.01	-	27.82	-	27.26	-	-	-
SwinIR [30]	×4	32.92	0.9044	29.09	0.7950	27.92	0.7489	27.45	0.8254	32.03	0.9260
SRFormer [72]	×4	32.93	0.9041	29.08	0.7953	27.94	0.7502	27.68	0.8311	32.21	0.9271
CAT-A [9]	×4	33.08	0.9052	29.18	0.7960	27.99	0.7510	27.89	0.8339	32.39	0.9285
MambaIR [20]	×4	33.03	0.9046	29.20	0.7961	27.98	0.7503	27.68	0.8287	32.32	0.9272
HAT [7]	×4	33.04	0.9056	29.23	0.7973	28.00	0.7517	27.97	0.8368	32.48	0.9292
ATD [65]	×4	33.10	0.9058	29.24	0.7974	28.01	0.7526	28.17	0.8404	32.62	0.9306
GRL [28]	×4	33.10	0.9094	29.37	0.8058	28.01	0.7611	28.53	0.8504	32.77	0.9325
MatIR (Ours)	×4	33.14	0.9055	29.40	0.8059	28.03	0.7610	28.55	0.8505	32.82	0.9326

restoration tasks, including image super-resolution and image denoising (*i.e.*, Gaussian color image denoising and real-world denoising), and Defocus deblurring results. (*i.e.*, S: single-image defocus deblurring. D: dual-pixel defocus deblurring). We employ DIV2K [49] and Flickr2K [32] to train classic SR models. Moreover, we use Set5 [5], Set14 [58], B100 [37], Urban100 [21], and Manga109 [38]

to evaluate the effectiveness of different SR methods. For gaussian color image denoising, we utilize DIV2K [49], Flickr2K [32], BSD500 [4], and WED [36] as our training datasets. Our testing datasets for gaussian color image denoising includes BSD68 [37], Kodak24 [18], McMaster [64], and Urban100 [21]. For real image denoising, we train our model with 320 high-resolution images from SIDD [1]



Figure 5. The visual comparison of the MatIR network on x2SR utilizes red bounding boxes to highlight the patch for comparison, in order to better reflect performance differences.

Table 5. **gaussian color image denoising** Quantitative comparison with state-of-the-art methods.

Method	BSD68			Kodak24			McMaster			Urban100		
	$\sigma=15$	$\sigma=25$	$\sigma=50$	$\sigma=15$	$\sigma=25$	$\sigma=50$	$\sigma=15$	$\sigma=25$	$\sigma=50$	$\sigma=15$	$\sigma=25$	$\sigma=50$
IRCNN [61]	33.86	31.16	27.86	34.69	32.18	28.93	34.58	32.18	28.91	33.78	31.20	27.70
FFDNet [62]	33.87	31.21	27.96	34.63	32.13	28.98	34.66	32.35	29.18	33.83	31.40	28.05
DnCNN [60]	33.90	31.24	27.95	34.60	32.14	28.95	33.45	31.52	28.62	32.98	30.81	27.59
DRUNet [63]	34.30	31.69	28.51	35.31	32.89	29.86	35.40	33.14	30.08	34.81	32.60	29.61
SwinIR [30]	34.42	31.78	28.56	35.34	32.89	29.79	35.61	33.20	30.22	35.13	32.90	29.82
Restormer [57]	34.40	31.79	28.60	35.47	33.04	30.01	35.61	33.34	30.30	35.13	32.96	30.02
MambaIR [20]	34.48	32.24	28.66	35.42	32.99	29.92	35.70	33.43	30.35	35.37	33.21	30.30
MatIR (Ours)	34.51	32.28	28.69	35.51	32.99	29.98	35.73	33.45	30.40	35.39	33.25	30.33

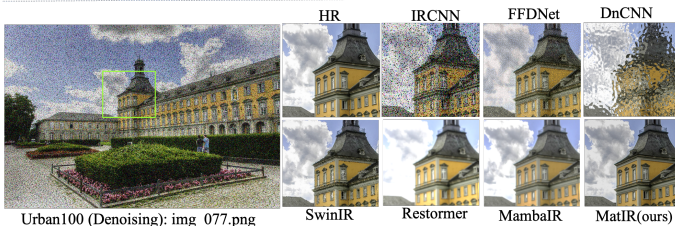
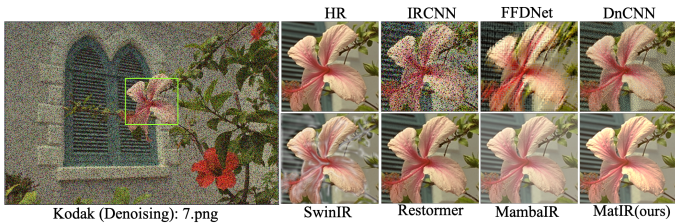


Figure 6. Visual comparisons between MatIR and state-of-the-art Denoising methods.

datasets, and use the SIDD test set and DND [44] dataset for testing. Following [30, 70], we denote the model as MatIR when self-ensemble strategy [32] is used in testing. The performance is evaluated using PSNR and SSIM on the Y channel from the YCbCr color space. Defocus Deblurring: We compare against 12 state-of-the-art methods on datasets comprising outdoor, indoor, and mixed scenes [2, 22, 27, 28, 48, 53, 57].

Training Details. In accordance with previous works [8, 30, 59], we perform data augmentation by applying horizontal flips and random rotations of 90° , 180° , and 270° . Additionally, we crop the original images into 64×64 patches for image SR and 128×128 patches for image denoising during training. For image SR, we use the pre-trained weights from the $\times 2$ model to initialize those of $\times 3$ and $\times 4$ and halve the learning rate and total training iterations to reduce training

time [32]. To ensure a fair comparison, we adjust the training batch size to 32 for image SR and 16 for image denoising. We employ the Adam [25] as the optimizer for training our MatIR with $\beta_1 = 0.9$, $\beta_2 = 0.999$. The initial learning rate is set at 2×10^{-4} and is halved when the training iteration reaches specific milestones. Our MatIR model is trained with 8 NVIDIA A100 GPUs.

Evaluation metrics. We use PSNR, SSIM, and LPIPS as the evaluation metrics for most image restoration tasks. In general, higher PSNR and SSIM, and lower LPIPS and FID mean better performance.

4.2. Ablation Study

Impact of different designs of Transformer Layer. As core components, TWLA and CGA can achieve higher quality image restoration for MatIR by activating more input pixels for local and global, triangular attention window and rectangular attention window ranges. In this section, we perform ablation studies on these two key components respectively. The results shown Tab. 1, Tab. 2: (1) Concatenating the two components in the Transformer Layer has a greater gain effect than using each component separately. (2) If the core component IRSS of the Mamba layer uses the Transformer method, the computational requirements will increase with the same benefit. Impact of different scanning modes in IRSS. In order for Mamba to process 2D images, the feature map needs to be flattened first and then iterated by the state space equation. Therefore, the unfolding strategy is particularly important. In this work, we follow [33] to generate scanning sequences using four different scanning directions. Here we ablate different scanning modes to study the effect, Compared with single-direction (upper left to lower right) and bidirectional (upper left to lower right, lower right to upper left) scanning, using four-directional scanning allows the anchor pixel to perceive a larger range of neighborhoods, thus achieving better results.

4.3. Evaluation on Image Super-Resolution

we compare our method with 16 state-of-the-art IR methods on 5 public datasets of classic super-resolution. The quantitative results are shown in Tab. 4. We can see that our method outperforms most of the methods on 5 different datasets. In particular, compared with the method SRformer, our method on Urban100 X4 leads SRformer by up to **0.87** on PSNR and leads DDNM by up to **0.0194dB** on SSIM. For qualitative results, our method has the best visual quality, including more realistic textures, as shown in Fig. 5. These visual comparisons are consistent with the quantitative results, demonstrating the effectiveness of our method. More visual results are placed in the supplementary material.

4.4. Evaluation on Image Denoising

The Gaussian color image denoising results are shown in Tab. 5. Similar to [60, 63], the compared noise levels in-

Table 6.

Defocus deblurring results. **S**: single-image defocus deblurring. **D**: dual-pixel defocus deblurring.

Method	Indoor Scenes				Outdoor Scenes				Combined			
	PSNR \uparrow	SSIM \uparrow	MAE \downarrow	LPIPS \downarrow	PSNR \uparrow	SSIM \uparrow	MAE \downarrow	LPIPS \downarrow	PSNR \uparrow	SSIM \uparrow	MAE \downarrow	LPIPS \downarrow
EBDB _S [22]	25.77	0.772	0.040	0.297	21.25	0.599	0.058	0.373	23.45	0.683	0.049	0.336
DMENet _S [26]	25.50	0.788	0.038	0.298	21.43	0.644	0.063	0.397	23.41	0.714	0.051	0.349
JNB _S [47]	26.73	0.828	0.031	0.273	21.10	0.608	0.064	0.355	23.84	0.715	0.048	0.315
DPDNet _S [2]	26.54	0.816	0.031	0.239	22.25	0.682	0.056	0.313	24.34	0.747	0.044	0.277
KPAC _S [48]	27.97	0.852	0.026	0.182	22.62	0.701	0.053	0.269	25.22	0.774	0.040	0.227
IFAN _S [27]	28.11	0.861	0.026	0.179	22.76	0.720	0.052	0.254	25.37	0.789	0.039	0.217
Restormer _S [57]	28.87	0.882	0.025	0.145	23.24	0.743	0.050	0.209	25.98	0.811	0.038	0.178
MatIR_S-B (Ours)	29.23	0.891	0.021	0.129	23.62	0.783	0.045	0.159	26.79	0.841	0.031	0.143
DPDNet _D [2]	27.48	0.849	0.029	0.189	22.90	0.726	0.052	0.255	25.13	0.786	0.041	0.223
RDPD _D [3]	28.10	0.843	0.027	0.210	22.82	0.704	0.053	0.298	25.39	0.772	0.040	0.255
Uformer _D [53]	28.23	0.860	0.026	0.199	23.10	0.728	0.051	0.285	25.65	0.795	0.039	0.243
IFAN _D [27]	28.66	0.868	0.025	0.172	23.46	0.743	0.049	0.240	25.99	0.804	0.037	0.207
Restormer _D [57]	29.48	0.895	0.023	0.134	23.97	0.773	0.047	0.175	26.66	0.833	0.035	0.155
MatIR_D-B (Ours)	30.16	0.911	0.019	0.093	24.70	0.817	0.039	0.123	27.83	0.862	0.029	0.105

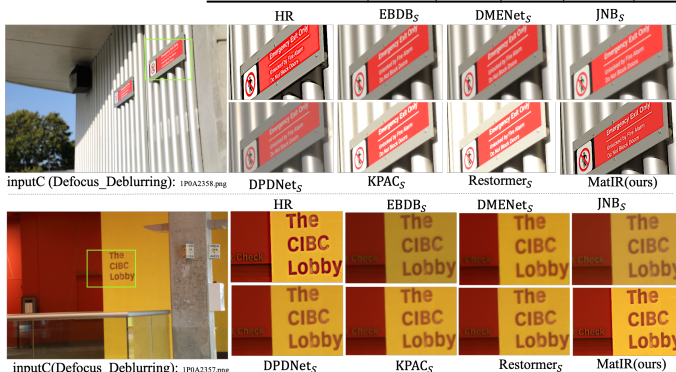


Figure 7. Visual comparisons between MatIR and state-of-the-art Defocus Deblurring methods.

clude 15, 25 and 50. It can be seen that our model achieves the best performance on most datasets. In particular, it surpasses SwinIR [30] and even reaches 0.51dB $\sigma=50$ on the Urban100 dataset. We also give a visual comparison in Figure 5. Benefiting from the global receptive field, our MatIR can achieve better structure preservation, resulting in clearer edges and natural shapes.

4.5. Evaluation on Image Deblurring

For image deblurring, we mainly evaluated the defocus deblurring results, including single image defocus deblurring and dual pixel defocus deblurring. In Table 5, the quantitative results show that our method achieves the best performance on all datasets. Compared with Outdoor Scenes by Restormer [57], the PSNR improvement of our method can be as high as **0.73dB**. The images we have the best visual quality, with more realistic details and close to GT images. Due to space limitations, we provide more quantitative and qualitative results in the supplementary materials.

4.6. Real Image Denoising.

We further turn to the real image denoising task to evaluate the robustness of MatIR in the face of real-world degradation. Following [57], we adopt a progressive training strategy for fair comparison. The results are shown in Tab. 7, showing that our method achieves the best performance among

Table 7. Quantitative comparison on the **real image denoising** task.

Dataset	DeamNet [46]		MPRNet [56]		Uformer [53]		Restormer [57]		MambaIR [20]		MatIR (Ours)	
	PSNR	SSIM	PSNR	SSIM	PSNR	SSIM	PSNR	SSIM	PSNR	SSIM	PSNR	SSIM
SIDD	39.47	0.957	39.71	0.958	39.77	0.959	40.02	0.960	39.89	0.960	40.08	0.963
DND	39.63	0.953	39.80	0.954	39.96	0.956	40.03	0.956	40.04	0.956	40.05	0.961

existing state-of-the-art models and outperforms other methods (such as Uformer [53]) by 0.31 dB PSNR on the SIDD dataset, demonstrating the capability of our method in real image denoising.

4.7. Further Experiments

Running time. We compare the running time of our proposed method with the SOTA IR method. For a fair comparison, we evaluate all methods on 256×256 input images on NVIDIA TITAN RTX using their publicly available codes. As shown in Tab. 3, the running time of the proposed method is significantly better than other transformer-based methods, demonstrating the good computational efficiency of our model.

5. Conclusion

In this paper, we introduce MatIR, a novel hybrid architecture for image restoration that combines the computational efficiency of the Mamba model with the powerful contextual learning capabilities of the Transformer. By leveraging the strengths of both architectures, MatIR is able to restore high-quality images at a lower computational cost. Extensive experiments on multiple image restoration tasks demonstrate that MatIR not only achieves state-of-the-art results in terms of PSNR and SSIM, but also achieves significant improvements in terms of memory efficiency and computational complexity. Our results suggest that hybrid architectures like MatIR offer a promising direction for advancing image restoration, especially in high-resolution and complex degraded scenes. Future work will explore extending this approach to video restoration tasks, where temporal dependencies will further benefit from the integration of SSM and Transformers.

References

- [1] Abdelrahman Abdelhamed, Stephen Lin, and Michael S Brown. A high-quality denoising dataset for smartphone cameras. In *Proceedings of the IEEE conference on computer vision and pattern recognition*, pages 1692–1700, 2018. 6
- [2] Abdullah Abuolaim and Michael S Brown. Defocus deblurring using dual-pixel data. In *Computer Vision–ECCV 2020: 16th European Conference, Glasgow, UK, August 23–28, 2020, Proceedings, Part X 16*, pages 111–126. Springer, 2020. 7, 8
- [3] Abdullah Abuolaim, Mauricio Delbracio, Damien Kelly, Michael S Brown, and Peyman Milanfar. Learning to reduce defocus blur by realistically modeling dual-pixel data. In *Proceedings of the IEEE/CVF International Conference on Computer Vision*, pages 2289–2298, 2021. 8
- [4] Pablo Arbelaez, Michael Maire, Charless Fowlkes, and Jitendra Malik. Contour detection and hierarchical image segmentation. *IEEE transactions on pattern analysis and machine intelligence*, 33(5):898–916, 2010. 6
- [5] Marco Bevilacqua, Aline Roumy, Christine Guillemot, and Marie Line Alberi-Morel. Low-complexity single-image super-resolution based on nonnegative neighbor embedding. 2012. 6
- [6] Hanting Chen, Yunhe Wang, Tianyu Guo, Chang Xu, Yiping Deng, Zhenhua Liu, Siwei Ma, Chunjing Xu, Chao Xu, and Wen Gao. Pre-trained image processing transformer. In *Proceedings of the IEEE/CVF conference on computer vision and pattern recognition*, pages 12299–12310, 2021. 1, 2, 6
- [7] Xiangyu Chen, Xintao Wang, Wenlong Zhang, Xiangtao Kong, Yu Qiao, Jiantao Zhou, and Chao Dong. Hat: Hybrid attention transformer for image restoration. *arXiv preprint arXiv:2309.05239*, 2023. 5, 6
- [8] Xiangyu Chen, Xintao Wang, Jiantao Zhou, Yu Qiao, and Chao Dong. Activating more pixels in image super-resolution transformer. In *Proceedings of the IEEE/CVF Conference on Computer Vision and Pattern Recognition*, pages 22367–22377, 2023. 1, 7
- [9] Zheng Chen, Yulun Zhang, Jinjin Gu, Yongbing Zhang, Linghe Kong, and Xin Yuan. Cross aggregation transformer for image restoration. In *NeurIPS*, 2022. 2, 5, 6
- [10] Zheng Chen, Yulun Zhang, Jinjin Gu, Linghe Kong, Xiaokang Yang, and Fisher Yu. Dual aggregation transformer for image super-resolution. In *Proceedings of the IEEE/CVF international conference on computer vision*, pages 12312–12321, 2023. 1
- [11] Xiangxiang Chu, Zhi Tian, Yuqing Wang, Bo Zhang, Haibing Ren, Xiaolin Wei, Huaxia Xia, and Chunhua Shen. Twins: Revisiting the design of spatial attention in vision transformers, 2021. 2
- [12] Tao Dai, Jianrui Cai, Yongbing Zhang, Shu-Tao Xia, and Lei Zhang. Second-order attention network for single image super-resolution. In *Proceedings of the IEEE/CVF conference on computer vision and pattern recognition*, pages 11065–11074, 2019. 1, 6
- [13] Tao Dai, Jianrui Cai, Yongbing Zhang, Shu-Tao Xia, and Lei Zhang. Second-order attention network for single image super-resolution. In *2019 IEEE/CVF Conference on Computer Vision and Pattern Recognition (CVPR)*, 2020. 2
- [14] Tri Dao and Albert Gu. Transformers are SSMS: Generalized models and efficient algorithms through structured state space duality. In *International Conference on Machine Learning (ICML)*, 2024. 2, 3
- [15] Xiaohan Ding, Xiangyu Zhang, Jungong Han, and Guiguang Ding. Scaling up your kernels to 31x31: Revisiting large kernel design in cnns. In *Proceedings of the IEEE/CVF conference on computer vision and pattern recognition*, pages 11963–11975, 2022. 1
- [16] Chao Dong, Chen Change Loy, Kaiming He, and Xiaoou Tang. Learning a deep convolutional network for image super-resolution. In *Computer Vision–ECCV 2014: 13th European Conference, Zurich, Switzerland, September 6–12, 2014, Proceedings, Part IV 13*, pages 184–199. Springer, 2014. 1, 2
- [17] Alexey Dosovitskiy. An image is worth 16x16 words: Transformers for image recognition at scale. *arXiv preprint arXiv:2010.11929*, 2020. 2
- [18] Rich Franzen. Kodak lossless true color image suite. 2021. 6
- [19] Albert Gu and Tri Dao. Mamba: Linear-time sequence modeling with selective state spaces. *arXiv preprint arXiv:2312.00752*, 2023. 2, 3
- [20] Hang Guo, Jinmin Li, Tao Dai, Zhihao Ouyang, Xudong Ren, and Shu-Tao Xia. Mambair: A simple baseline for image restoration with state-space model. In *European Conference on Computer Vision*, pages 222–241. Springer, 2025. 3, 6, 7, 8
- [21] Jia-Bin Huang, Abhishek Singh, and Narendra Ahuja. Single image super-resolution from transformed self-exemplars. In *Proceedings of the IEEE conference on computer vision and pattern recognition*, pages 5197–5206, 2015. 6
- [22] Ali Karaali and Claudio Rosito Jung. Edge-based defocus blur estimation with adaptive scale selection. *IEEE Transactions on Image Processing*, 27(3):1126–1137, 2017. 7, 8
- [23] Jiwon Kim, Jung Kwon Lee, and Kyoung Mu Lee. Accurate image super-resolution using very deep convolutional networks. In *2016 IEEE Conference on Computer Vision and Pattern Recognition (CVPR)*, 2016. 2
- [24] Jiwon Kim, Jung Kwon Lee, and Kyoung Mu Lee. Deeply-recursive convolutional network for image super-resolution. In *Proceedings of the IEEE conference on computer vision and pattern recognition*, pages 1637–1645, 2016. 2
- [25] Diederik P Kingma and Jimmy Ba. Adam: A method for stochastic optimization. *arXiv preprint arXiv:1412.6980*, 2014. 7
- [26] Junyong Lee, Sungkil Lee, Sunghyun Cho, and Seungyong Lee. Deep defocus map estimation using domain adaptation. In *Proceedings of the IEEE/CVF conference on computer vision and pattern recognition*, pages 12222–12230, 2019. 8
- [27] Junyong Lee, Hyeongseok Son, Jaesung Rim, Sunghyun Cho, and Seungyong Lee. Iterative filter adaptive network for single image defocus deblurring. In *Proceedings of the IEEE/CVF Conference on Computer Vision and Pattern Recognition*, pages 2034–2042, 2021. 7, 8
- [28] Yawei Li, Yuchen Fan, Xiaoyu Xiang, Denis Demandolx, Rakesh Ranjan, Radu Timofte, and Luc Van Gool. Efficient

- and explicit modelling of image hierarchies for image restoration. In *Proceedings of the IEEE/CVF Conference on Computer Vision and Pattern Recognition*, pages 18278–18289, 2023. 4, 6, 7
- [29] Yawei Li, Yuchen Fan, Xiaoyu Xiang, Denis Demandolx, Rakesh Ranjan, Radu Timofte, and Luc Van Gool. Efficient and explicit modelling of image hierarchies for image restoration. In *Proceedings of the IEEE/CVF Conference on Computer Vision and Pattern Recognition*, pages 18278–18289, 2023. 1, 2
- [30] Jingyun Liang, Jiezhong Cao, Guolei Sun, Kai Zhang, Luc Van Gool, and Radu Timofte. Swinir: Image restoration using swin transformer. In *Proceedings of the IEEE/CVF international conference on computer vision*, pages 1833–1844, 2021. 1, 2, 4, 5, 6, 7, 8
- [31] Bee Lim, Sanghyun Son, Heewon Kim, Seungjun Nah, and Kyoung Mu Lee. Enhanced deep residual networks for single image super-resolution. In *2017 IEEE Conference on Computer Vision and Pattern Recognition Workshops (CVPRW)*, 2017. 2
- [32] Bee Lim, Sanghyun Son, Heewon Kim, Seungjun Nah, and Kyoung Mu Lee. Enhanced deep residual networks for single image super-resolution. In *Proceedings of the IEEE conference on computer vision and pattern recognition workshops*, pages 136–144, 2017. 1, 6, 7
- [33] Yue Liu, Yunjie Tian, Yuzhong Zhao, Hongtian Yu, Lingxi Xie, Yaowei Wang, Qixiang Ye, and Yunfan Liu. Vmamba: Visual state space model. *arXiv preprint arXiv:2401.10166*, 2024. 1, 2, 3, 7
- [34] Ze Liu, Yutong Lin, Yue Cao, Han Hu, Yixuan Wei, Zheng Zhang, Stephen Lin, and Baining Guo. Swin transformer: Hierarchical vision transformer using shifted windows. In *Proceedings of the IEEE/CVF international conference on computer vision*, pages 10012–10022, 2021. 2
- [35] Wenjie Luo, Yujia Li, Raquel Urtasun, and Richard Zemel. Understanding the effective receptive field in deep convolutional neural networks. *Advances in neural information processing systems*, 29, 2016. 1
- [36] Kede Ma, Zhengfang Duanmu, Qingbo Wu, Zhou Wang, Hongwei Yong, Hongliang Li, and Lei Zhang. Waterloo exploration database: New challenges for image quality assessment models. *IEEE Transactions on Image Processing*, 26(2):1004–1016, 2016. 6
- [37] David Martin, Charless Fowlkes, Doron Tal, and Jitendra Malik. A database of human segmented natural images and its application to evaluating segmentation algorithms and measuring ecological statistics. In *Proceedings Eighth IEEE International Conference on Computer Vision. ICCV 2001*, pages 416–423. IEEE, 2001. 6
- [38] Yusuke Matsui, Kota Ito, Yuji Aramaki, Azuma Fujimoto, Toru Ogawa, Toshihiko Yamasaki, and Kiyoharu Aizawa. Sketch-based manga retrieval using manga109 dataset. *Multi-media Tools and Applications*, 76:21811–21838, 2017. 6
- [39] Yiqun Mei, Yuchen Fan, Yuqian Zhou, Lichao Huang, Thomas S Huang, and Honghui Shi. Image super-resolution with cross-scale non-local attention and exhaustive self-exemplars mining. In *Proceedings of the IEEE/CVF conference on computer vision and pattern recognition*, pages 5690–5699, 2020. 2, 6
- [40] Yiqun Mei, Yuchen Fan, and Yuqian Zhou. Image super-resolution with non-local sparse attention. In *2021 IEEE/CVF Conference on Computer Vision and Pattern Recognition (CVPR)*, 2021. 2
- [41] Yiqun Mei, Yuchen Fan, and Yuqian Zhou. Image super-resolution with non-local sparse attention. In *Proceedings of the IEEE/CVF Conference on Computer Vision and Pattern Recognition*, pages 3517–3526, 2021. 6
- [42] Ben Niu, Weilei Wen, Wenqi Ren, Xiangde Zhang, Lianping Yang, Shuzhen Wang, Kaihao Zhang, Xiaochun Cao, and Haifeng Shen. *Single Image Super-Resolution via a Holistic Attention Network*, page 191–207. 2020. 2
- [43] Ben Niu, Weilei Wen, Wenqi Ren, Xiangde Zhang, Lianping Yang, Shuzhen Wang, Kaihao Zhang, Xiaochun Cao, and Haifeng Shen. Single image super-resolution via a holistic attention network. In *Computer Vision–ECCV 2020: 16th European Conference, Glasgow, UK, August 23–28, 2020. Proceedings, Part XII 16*, pages 191–207. Springer, 2020. 6
- [44] Tobias Plotz and Stefan Roth. Benchmarking denoising algorithms with real photographs. In *Proceedings of the IEEE conference on computer vision and pattern recognition*, pages 1586–1595, 2017. 7
- [45] Abhisek Ray, Gaurav Kumar, and Maheshkumar H Kolekar. Cfat: Unleashing triangular windows for image super-resolution. *arXiv preprint arXiv:2403.16143*, 2024. 2, 3, 4
- [46] Chao Ren, Xiaohai He, Chuncheng Wang, and Zhibo Zhao. Adaptive consistency prior based deep network for image denoising. In *Proceedings of the IEEE/CVF conference on computer vision and pattern recognition*, pages 8596–8606, 2021. 8
- [47] Jianping Shi, Li Xu, and Jiaya Jia. Just noticeable defocus blur detection and estimation. In *Proceedings of the IEEE Conference on Computer Vision and Pattern Recognition*, pages 657–665, 2015. 8
- [48] Hyeonseok Son, Junyong Lee, Sunghyun Cho, and Seungyong Lee. Single image defocus deblurring using kernel-sharing parallel atrous convolutions. In *Proceedings of the IEEE/CVF International Conference on Computer Vision*, pages 2642–2650, 2021. 7, 8
- [49] Radu Timofte, Eirikur Agustsson, Luc Van Gool, Ming-Hsuan Yang, and Lei Zhang. Ntire 2017 challenge on single image super-resolution: Methods and results. In *Proceedings of the IEEE conference on computer vision and pattern recognition workshops*, pages 114–125, 2017. 6
- [50] Roger Waleffe, Wonmin Byeon, Duncan Riach, Brandon Norick, Vijay Korthikanti, Tri Dao, Albert Gu, Ali Hatamizadeh, Sudhakar Singh, Deepak Narayanan, et al. An empirical study of mamba-based language models. *arXiv preprint arXiv:2406.07887*, 2024. 2, 3, 5
- [51] Hang Wang, Xuanhong Chen, Bingbing Ni, Yutian Liu, and Liu jinfan. Omni aggregation networks for lightweight image super-resolution. In *Conference on Computer Vision and Pattern Recognition*, 2023. 2

- [52] Wenhai Wang, Enze Xie, Xiang Li, Deng-Ping Fan, Kaitao Song, Ding Liang, Tong Lu, Ping Luo, and Ling Shao. Pyramid vision transformer: A versatile backbone for dense prediction without convolutions. In *2021 IEEE/CVF International Conference on Computer Vision (ICCV)*, 2022. [2](#)
- [53] Zhendong Wang, Xiaodong Cun, Jianmin Bao, Wengang Zhou, Jianzhuang Liu, and Houqiang Li. Uformer: A general u-shaped transformer for image restoration. In *Proceedings of the IEEE/CVF Conference on Computer Vision and Pattern Recognition (CVPR)*, pages 17683–17693, 2022. [7](#), [8](#)
- [54] Juan Wen, Shupeng Cheng, Peng Xu, Bowen Zhou, Radu Timofte, Weiyan Hou, and Luc Van Gool. When super-resolution meets camouflaged object detection: A comparison study. *arXiv preprint arXiv:2308.04370*, 2023. [1](#), [2](#), [4](#)
- [55] Juan Wen, Yawei Li, Chao Zhang, Weiyan Hou, Radu Timofte, and Luc Van Gool. Empowering image recovery- a multi-attention approach. *arXiv preprint arXiv:2404.04617*, 2024. [1](#), [2](#), [4](#)
- [56] Syed Waqas Zamir, Aditya Arora, Salman Khan, Munawar Hayat, Fahad Shahbaz Khan, Ming-Hsuan Yang, and Ling Shao. Multi-stage progressive image restoration. In *Proceedings of the IEEE/CVF conference on computer vision and pattern recognition*, pages 14821–14831, 2021. [8](#)
- [57] Syed Waqas Zamir, Aditya Arora, Salman Khan, Munawar Hayat, Fahad Shahbaz Khan, and Ming-Hsuan Yang. Restormer: Efficient transformer for high-resolution image restoration. In *Proceedings of the IEEE/CVF conference on computer vision and pattern recognition*, pages 5728–5739, 2022. [7](#), [8](#)
- [58] Roman Zeyde, Michael Elad, and Matan Protter. On single image scale-up using sparse-representations. In *Curves and Surfaces: 7th International Conference, Avignon, France, June 24-30, 2010, Revised Selected Papers 7*, pages 711–730. Springer, 2012. [6](#)
- [59] Jiale Zhang, Yulun Zhang, Jinjin Gu, Yongbing Zhang, Linghe Kong, and Xin Yuan. Accurate image restoration with attention retractable transformer. In *ICLR*, 2023. [2](#), [5](#), [7](#)
- [60] Kai Zhang, Wangmeng Zuo, Yunjin Chen, Deyu Meng, and Lei Zhang. Beyond a gaussian denoiser: Residual learning of deep cnn for image denoising. *IEEE transactions on image processing*, 26(7):3142–3155, 2017. [1](#), [7](#)
- [61] Kai Zhang, Wangmeng Zuo, Shuhang Gu, and Lei Zhang. Learning deep cnn denoiser prior for image restoration. In *Proceedings of the IEEE conference on computer vision and pattern recognition*, pages 3929–3938, 2017. [7](#)
- [62] Kai Zhang, Wangmeng Zuo, and Lei Zhang. Ffdnet: Toward a fast and flexible solution for cnn-based image denoising. *IEEE Transactions on Image Processing*, 27(9):4608–4622, 2018. [7](#)
- [63] Kai Zhang, Yawei Li, Wangmeng Zuo, Lei Zhang, Luc Van Gool, and Radu Timofte. Plug-and-play image restoration with deep denoiser prior. *IEEE Transactions on Pattern Analysis and Machine Intelligence*, 44(10):6360–6376, 2021. [7](#)
- [64] Lei Zhang, Xiaolin Wu, Antoni Buades, and Xin Li. Color demosaicking by local directional interpolation and nonlocal adaptive thresholding. *Journal of Electronic imaging*, 20(2):023016–023016, 2011. [6](#)
- [65] Leheng Zhang, Yawei Li, Xingyu Zhou, Xiaorui Zhao, and Shuhang Gu. Transcending the limit of local window: Advanced super-resolution transformer with adaptive token dictionary. In *Proceedings of the IEEE/CVF Conference on Computer Vision and Pattern Recognition*, pages 2856–2865, 2024. [6](#)
- [66] Xindong Zhang, Hui Zeng, Shi Guo, and Lei Zhang. Efficient long-range attention network for image super-resolution. In *European Conference on Computer Vision*, pages 649–667. Springer, 2022. [2](#), [6](#)
- [67] Yulun Zhang, Kungpeng Li, Kai Li, Lichen Wang, Bineng Zhong, and Yun Fu. Image super-resolution using very deep residual channel attention networks. In *Proceedings of the European conference on computer vision (ECCV)*, pages 286–301, 2018. [6](#)
- [68] Yulun Zhang, Kungpeng Li, Kai Li, Lichen Wang, Bineng Zhong, and Yun Fu. *Image Super-Resolution Using Very Deep Residual Channel Attention Networks*, page 294–310. 2018. [2](#)
- [69] Yulun Zhang, Yapeng Tian, Yu Kong, Bineng Zhong, and Yun Fu. Residual dense network for image super-resolution, 2018. [2](#)
- [70] Yulun Zhang, Yapeng Tian, Yu Kong, Bineng Zhong, and Yun Fu. Residual dense network for image super-resolution. In *Proceedings of the IEEE conference on computer vision and pattern recognition*, pages 2472–2481, 2018. [1](#), [7](#)
- [71] Shangchen Zhou, Jiawei Zhang, Wangmeng Zuo, and Chen Change Loy. Cross-scale internal graph neural network for image super-resolution. In *Advances in Neural Information Processing Systems*, 2020. [6](#)
- [72] Yupeng Zhou, Zhen Li, Chun-Le Guo, Song Bai, Ming-Ming Cheng, and Qibin Hou. Srformer: Permuted self-attention for single image super-resolution. *arXiv preprint arXiv:2303.09735*, 2023. [6](#)